Journal of Mining and Environment (JME), Vol. 14, No. 1, 2023, 277-293

Shahrood University of Technology

Journal of Mining and Environment (JME)

Journal homepage: www.jme.shahroodut.ac.ir

Iranian Society of Mining Engineering (IRSME)

Mineralogy and Characterisation Studies Aimed at Coal Desulfurization Process on Iran's Largest Coalfield

Sajjad Jannesar Malakooti[1*], Hadi Abdollahi[2], Ziaeddin Pourkarimi[3], Behrouz Karimi Shahraki[3], Mehdi Rahimi[3], Mohammadreza Shahbazi[2], and Ahmad Rahmanian kooshkaki[2]

1. Tabas Coal Mines Complex (TCMC), Iranian Mines & Mining Industries Development & Renovation Organization (IMIDRO), Tabas, Iran
2. School of Mining, College of Engineering, University of Tehran, Tehran, Iran
3. Iran Mineral Processing Research Center (IMPRC), Iran

Article Info

Received 19 December 2022
Received in Revised form 5 February 2023
Accepted 28 February 2023
Published online 28 February 2023

DOI:10.22044/jme.2023.12529.2274

Keywords

Coal mineralogy
Coal desulfurization
Framboidal pyrite
Coal washing plants

Abstract

Parvadeh IV and East Parvadeh mines are two main coal-producing zones within the Tabas coalfield, east of Iran. Since studies have shown that C1 and B2 are the most important working seams in the Parvadeh IV and east Parvadeh areas, this research work focuses on these two coal seams. Syngenetic pyrite is available as framboids related to macerals. Decreasing the sulfur content is especially hard when the pyrite particles are fine-grained, finely disseminated, and intergrown with the coal maceral structure. The sulfur content measured in C1 and B2 seams varies from 0.98% to 5.57% and from 0.73% to 5.25%, respectively, with an average of 2.39% and 2.5%. We use a method to predict how coal desulfurized the C1-and B2-seams of Parvadeh IV and C1 seams of east Parvadeh mines in the Tabas coalfield. The results have given new proofs for the presence of pyrite and clay minerals within the coalfield zone, and to identify a method to predict coal desulfurization with conventional processing and cost-effective methods. The coal preparation strategy in MEMRADCO, Parvadeh, and Ehyasepahan coal-cleaning plants not as it expels mineral matter and pyrite but too reduces the content of most inorganic components.

1. Introduction

Coal is a combustible, black or brownish-black sedimentary rock that forms in coal seams. A significant impediment related to utilizing coal is the emanation of sulfur dioxide into the environment during combustion. These natural impacts associated with coal combustion have driven the advancement of previously unused forms to control the discharging emanation [1]. With the expanded intrigue in maintaining a strategic distance from the negative impacts of coal utilization and combustion and on the recuperation of primary components from coal and coal combustion by-products, the essential and mineralogical compositions of coal are one of the foremost examined subjects in coal washing technology [1-5]. Coal comprises two sorts of materials: macerals and inorganic compounds. From a hereditary viewpoint, the minerals in coal, like the natural matter, are the item of the forms related to peat collection and rank progress, as well as the interaction of the biological matter with basinal liquids and sediment diagenesis. Coal minerals comprise quartz, clay, carbonate, and sulfide minerals [6]. In later decades, one of the drawbacks related to utilizing coal as a source of vitality in combustion frameworks was the outflow of sulfur oxides and hydrogen sulfide into the environment. These issues have driven the use of fluidized bed combustion and vent gas desulfurization forms within the industry to control sulfur release [7]. The minerals are the essential source of fly ash particles, ash, and slag and contribute to flue-gas desulfurization [5]. Micro-structural highlights may influence the determination of coal beneficiation strategies for expelling pollution. For illustration, in arranging sulfur expulsion plans, it is valuable to get the proportionment of inorganic sulfur compared with

Corresponding author: s.jannesar114@gmail.com (S. Jannesar Malakooti)

that of organic sulfur. The size, shape, orientation, and dispersion variables for pyrite and maceral groupings (macerals and other organic components) are significant in supporting judicious plans of sulfur expulsion forms [8]. Pyrite within the Tabas area shows up as framboidal totals. The inorganic sulfur is shown primarily in pyrite and sulfate shapes [7, 9]. Sulfides can be categorized as syngenetic (essential), early diagenetic, or epigenetic (secondary) in the beginning. Syngenetic pyrite is shaped amid amassing of the peat and/or amid early (humification) forms and is ordinarily fine and scattered within the coal [1, 3, 10-12].

In the coke-making process, the coal mineral components such as apatite and pyrite release heavy substances such as phosphorus and sulfur, which cause the generation of poor-quality iron [13]. The transformation of quartz to cristobalite within the coke may break and damage it. Calcium- and Fe-bearing minerals may also influence coke reactivity. Reducing the sulfur content of coal is exceptionally troublesome when the pyrite grains are tiny, finely spread, and intergrown with the coal [10]. If the grains appear coarse and not intergrown after pulverizing, there is a higher chance of concentrating the pyrite within the residue [5]. The estimate and dispersion of pyrite determine the simple strategy of ordinary coal arrangement utilized and, concurrently, the amount of pyrite that can be expelled. Minerals like pyrite, which have higher densities than coal itself play a big role in the division [14].

The main goal of this work is to investigate the mineralogical composition of the three sample types of Parvadeh coalfield, the dominant minerals and crystallography by using microscopic and liberation degree studies, petrography, and scanning electron microscope studies. Therefore, we can make better decisions regarding the desulfurization of parvadeh coal.

2. Materials and method

2.1. Geological setting

The Tabas Coalfield, with a range of over 30,000 square kilometers and an exploratory reserve of 6 billion tons of coking and thermal coal, is the richest and largest coalfield in Iran. It is augmented in the Parvadeh, Nayband, Abdughi, and Mazino districts (Figure S1 and Table 1). Parvadeh has a surface area of around 1200 km^2, and is located 75–115 km south of Tabas (South Khorasan Province of Iran). Triassic and Jurassic deposits have developed middling heights in the south, while the northern zone comprises plains and salt marshes. Shotory heights bound the region to the east and Kamarmahdi heights to the west. The Mesozoic era is the age of Iranian coking coals (Late Triassic–Middle Jurassic). These coals have coking qualities, a high ash level, and a high sulfur content. [15]. There are two types of reserves in coal deposits (thermal and coking coals). The nation's total coal reserves are around 11 billion tons. Greater than 76% of the nation's coal deposits are located in the Tabas region (Table 1 and Figure S1). The deposits at Parvadeh and Naiband consist of coking coal. In contrast, those at Mazino and Abdoughi consist of thermal coal. More than 76% of Iran's coal deposits are located in the Tabas region (Table 1) [16].

Table 1. Reserves of different blocks in Tabas Coalfield.

Area	Distance to Tabas	Proved and Probable explored reserves (million tons)	
Parvadeh	75 Km to the south	1100	Coking coal
Naiband	200 Km to the south east	200	Coking coal
Mazino	75 Km to the west	1400	Thermal coal
Abdoughi	South west	Under exploration	Thermal coal

The Tabas coalfield is located in the center region of the Tabas basin, which is separated from Yazd and Lut Blocks by the Nayband to the east and the Kalmard-Kouhbanan faults to the west [17]. The Tabas block consists of five key coalfields: Parvadeh, Nayband, Mazino, Abdooghi, and Kalshaneh [15]. A substantial portion of the Tabas Block consists of the upper Triassic to the Middle Cretaceous. The most major coal-bearing layers in the Tabas were formed during the Late Triassic and Middle Jurassic inside the Shemshak Group [17-19].

Approximately 80 km south of the Tabas area in Central Iran is the East-Parvadeh coal resource (Figure S1). The Parvadeh region is split into six sections by significant faults. The Zenoughan fault divides the East-Parvadeh coal deposit (Figure S1) into the North and South Blocks. According to the coal seams' dip, depth, and structural impacts, the North Block is preferable to the South Block. The

Nayband formation and Ghadir component of the Tabas coalfield's coal-bearing layers contain sediments from the Upper Triassic and Middle Jurassic eras. Among the rock types, siltstone, sandstone, shale, sandy siltstone, and trace quantities of limestone and ash coal could be found. The Parvadeh district named its seams A, B, C, D, E, and F. The B and C seams are deemed mineable based on their quality and quantity, notably C1 and B2 [20]. This depositional layer may represent a section of the Nayband. The Rostam, Quri-Chay, and Zenowghan faults define the northern, southern, and central-western boundaries of Parvadeh, respectively. Based on these faulting processes, the Parvadeh zone may be divided into six sub-regions, with Parvadeh IV being the most advantageous due to the quantity and quality of its coal deposits. The primary coal seams of the Parvadeh region are named B1, B2, C1, C2, and D (Figure S2) (A, B, and C, respectively).

2.2. Samples and analytical procedures

The Alborz-based Iran Mineral Processing Research Center (IMPRC) conducted all analyses for this work. Silica, gypsum, and pyrite infill coal samples. The top seam contains more coal lithotypes gelified with humic amorphous, while the lower seam contains mineral-rich coals with clayey bands thicker than 1 mm. East Parvadeh, Block 4 (C1 seam), and Block 4 (B2 seam) mines provided coal samples. After IMPRC coding, the 2100 kg samples were split into 288 kg control samples. In order to avoid contamination and oxidation, the samples were immediately stored in clean plastic packets. After being coded by the IMPRC, each coal sample was delivered as a control sample by network sampling. A typical sample was taken from the region's mines. The representative samples were prepared for the subsequent study using sampling methods including Jones riffles, conning, and quartering [7]. After coning and quartering the representative sample of 108 kg, particles bigger than 38 mm were crushed and reduced to a fraction of less than 38 mm to prepare the coal samples for mineralogy investigations (part I), processing tests, and sulfur and ash analysis. Both wet and dry sieves were evaluated for mineralogy, processing, and ash and sulfur analysis, with fraction ranges of -0.5, -2 + 0.5, -10 + 2, and -38 + 10 mm. Ash and sulfur analyses used ASTM-D3174 and D3177 standards. Table S1 shows the ASTM proximate analyses (ASTM D3173-11, 2011; D3174-11, 2011; and D3175-11, 2011). ASTM analyzed total sulfur and sulfur types (ASTM D3177–02, 2011; ASTM D2492–02, 2002) [21]. The sample procedure was implemented based on coal seam compositions at the underground mining stops at Parvadeh No. IV and east Parvadeh mines in the Parvadeh area. The coal's rank is determined using approximate analysis to show the proportion of combustible to incombustible constituents [21]. ASTM D3172-76 is used for the proximate and ultimate analysis of coal samples [22]. Results of the relative analysis, forms of sulfur, and vitrinite reflectance of the Parvadeh coal mines are given in Table 2 and Table S2 summarizes the sampling performed for the study.

Table 2. Characterization of C1 and B2 coal seams of the Parvadeh area.

Seam	Value	Proximate analysis (wt% as received)					P(%)	P.I (%)		∑OR
		M	A	V.M	F.C	ST		X	Y	
C1	Min-max	0.3-1.3	8-30	22.3-34.7	51.7	0.25- 4.75	0.001-0.033	-10-24	10-25	94-103
	Ave.	0.8	19	28.5		2.50	0.017	5.6	17	99
B2	Min-max	0.2-1.6	13-40	19.6-34.6	45.5	0.93-5.25	0-0.091	-14-17	8-22	97-103
	Ave.	0.9	26.5	27.1		3.09	0.045	11	16	99

M: Moisture, A: Ash, V.M: Volatile Matter, F.C: Fixed Carbon, ST: Total Sulfur, P: Phosphor, P.I: Plostometry Index.

Standard proximate and ultimate analyses and calorific values of the coal samples were performed utilizing the TGA-601, LECO SC-144DR, and AC-350 furnaces separately by the ASTM method. This equipment was calibrated using standard materials for coal from the LECO Company. For mineralogical and petrographical analyses, the coal samples were prepared according to ASTM D2797/D2797M (2011) with -1 mm sample fractions. They were inspected utilizing transmitted-reflected polarizing light microscopy (ZEISS Axioplan 2). Maceral identification was applied by the International Committee for Coal Petrology (ICCP, 2001). The mineral compositions were determined employing a polarized light microscope (PLM), showing no. Axioplan2 of ZEISS Co. Thin sections (n = 20), polished thin sections (n = 10), and polished sections (n = 10)

were prepared for petrographic investigations and were done under a Zeiss Axioscope optical microscope. Ash samples were ground to 70 μm and analyzed by X-ray diffraction (XRD). XRD investigations were performed with a Philips Xpert-Pro, utilizing Co Kα1(1.789010 Å) radiation, monochromators on secondary optics, 40 kV of control, and 35- mA of current at the IMPRC. A scanning electron microscope (SEM) and an EDX (energy-dispersive X-ray spectrometer) were used to figure out what kind of minerals were being looked at at the IMPRC under an LEO 1450.

3. Results and Discussion

3.1. Iso-Sulfur curves

The sulfur content of coals in the Parvadeh region is highly variable and varies with seams. The amount of sulfur usually decreases from the west to the east of Parvadeh. This current work focuses on two significant and workable stops, the C1 and B2 seams. Most of these changes in sulfur content are associated with synthetic sulfur, which is similar to the plant. In all Parvadeh areas, epigenetic sulfurs, especially pyrite and marcasite, are similar. In the samples of coal seams in each area, pyrite, the main mineral, is present in the form of cavity filling for primary and secondary micro-cracks. In the following, changes in sulfur in the Parvadeh coal seams are investigated. The amount of sulfur measured in the C1 and B2 seams varies from 0.98% to 5.57% and from 0.73% to 5.25%, with an average of 2.39% and 2.5%, respectively. In the classification of coals based on sulfur content, the C1 and B2 seams belong to the "moderate" to "high sulfur" category of coals. Figure 1 (A and B) shows the iso-sulfur curve for the C1 and B2. Most of the sulfur in the B2 coal seam is synthetic and cannot be separated from the conventional coal-washing process. Considering that in the coal concentrate sample, the amount of sulfur is reduced by a maximum of 40%, the amount of sulfur in the concentrate will be about 1.5–3 %, which will play a key role in the problems of converting coal to coke.

3.2. Iso-Ash curves

The ash content in the samples taken from the Parvadeh area is different for each coal seam. In many cases, the ash content is different, and the range of changes is varied in each coal seam. To study the ash content in the Parvadeh coalfield, the ash in each coal seam was first measured, and then the iso-ash curves were prepared according to the general changes in the characteristics of the coal in the whole area. Ash measurements were mainly performed on workable coal seams. The total ash of the C1 and B2 seams is at least 7.7% and 13.4%, with a maximum of 45.1% and 39.8%, and an average of 18.57% and 26.4%, which is without non-coal seams. In coal branches, the minimum ash content is 7.7%, the maximum is 34.6%, and the average is 18.03%, respectively. These layers are classified as "medium and relatively high" ash in the classification of coals based on ash content. Due to the amount of ash and the range of changes, these seams are categorized as bituminous coal. Figure 1 (C and D) shows the iso-ash curve of the C1 and B2 coal seams.

3.3. Iso-Thickness curves

C1's head is located 23.5 m away from B2, and its bottom is 11 m below the C2 seam. In terms of coal structure, this coal seam is the most stable layer of coal in the Parvadeh area. In almost all boreholes drilled in this layer, it is seen as a branch of lump coal with high hardness. Figure 2 (A and B) shows the full specifications of the seams including the thickness of the C1 and B2 seams. The thickness of the non-coal seam decreases from west to east, and the number of coal branches decreases so that sometimes it includes only one part. B2 is located in the Parvadeh at a distance of approximately 9.5 m from B1 at the bottom, and 23.5 m below C1. The floor of B2 is made of siltstone with a maximum thickness of 25 cm and then Arcos gray sandstone. The B2 coal seam is lumpy and shiny and does not break easily. There was less pyrite and marcasite in the samples, and most of the cracks were filled with calcite and clay.

According to Figure 2 (A and B), the minimum, maximum, and average thickness of the C1 and B2 seams are, in the Parvadeh area, 0.4, 0.4, 1.15, 2, and 0.9, 1.05 m, respectively. Simple minerals and composite structures exist in all boreholes in the C1 and B2 seams. Also the thickness of the non-coal seams varies between 0.25 and 0.5 m for the C1 seam and 0.5 and 1.9 m for the B2 seam. C1 did not show workable thickness in 40 boreholes and suitable thickness in 9 boreholes, which means that this layer has a workable thickness in more than 81% of boreholes and below +611 m, and the B2 seam can be used in approximately 80% of boreholes and below the +600 level. As mentioned earlier, these seams are categorized as "medium" ash content and "moderate" to "high sulfur" in the sulfur content. Based on Figure 2 (A and B), the following results are obtained for the C1 and B2 coal seams: the average thickness of coal branches

in the B2 seam is 0.9 m; the thickness is workable in 139 boreholes, which were more than 40 cm. 49 new boreholes were drilled at this stage, 39 of them were workable, and ten boreholes do not show suitable thickness. This means that B2 can be used in approximately 80% of boreholes below the +600 level.

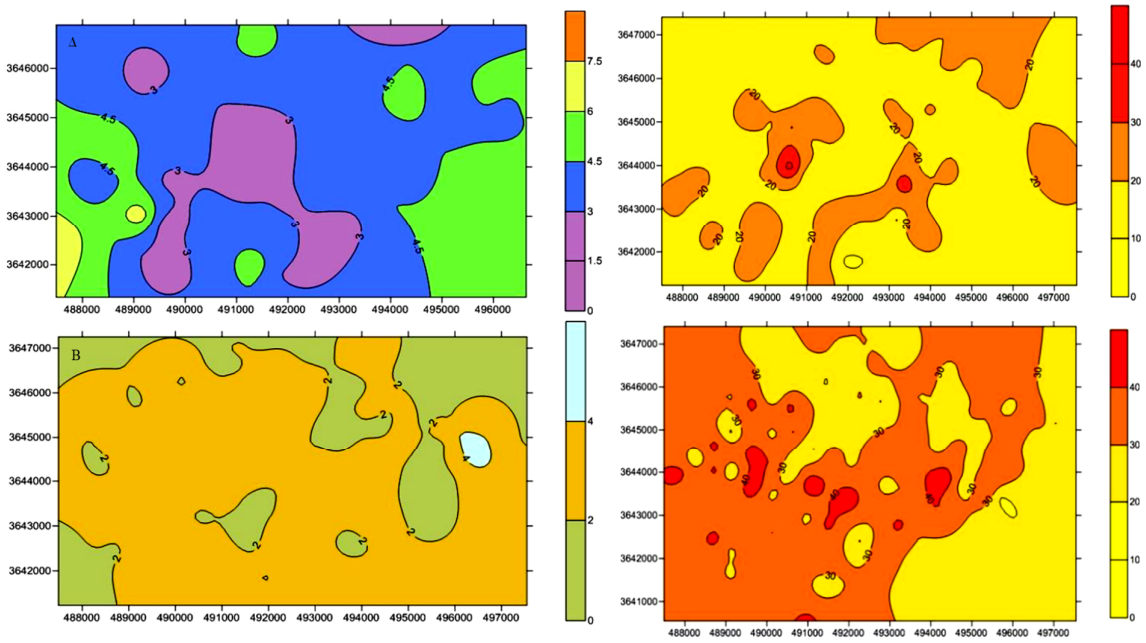

Figure 1. (A and B): Iso-Sulfur curves and (C and D): Iso-Ash curves for C1 and B2 coal seams of Parvadeh area.

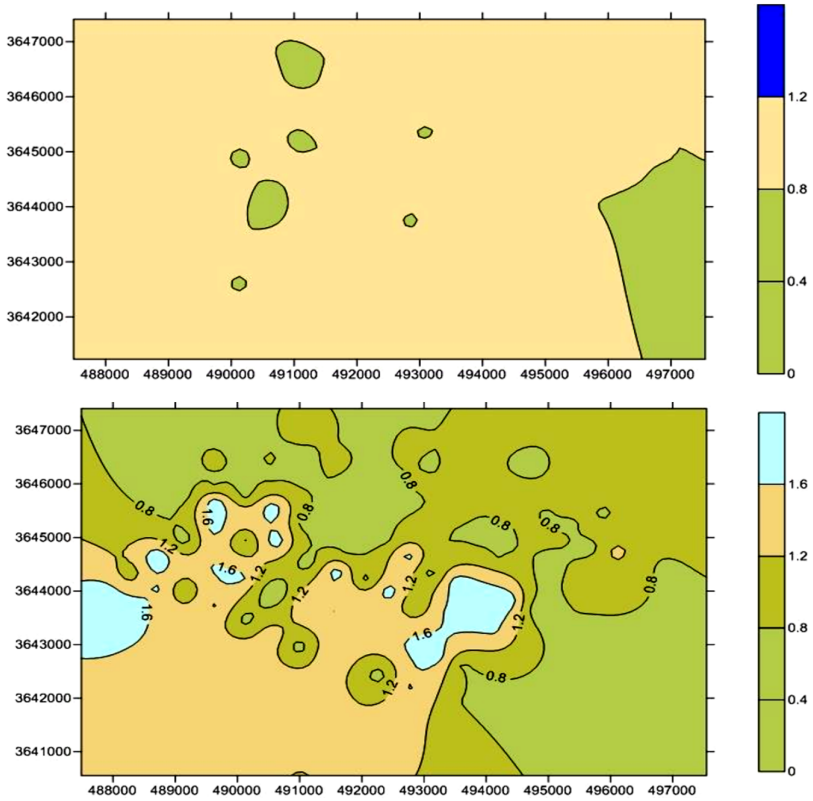

Figure 2. (A and B): Iso-Thickness curves for C1 and B2 coal seams of the Parvadeh area.

3.4. Mineralogical studies

3.4.1. Microscopic and Liberation degree studies

Table S3 shows ash and sulfur content values (total sulfur, pyrite, sulfate, and organic) measured in fractional sizes and calculating the amount of sulfur (total sulfur, pyrite, sulfate, and organic) and the entire ash content of the C1 seam of eastern Parvadeh (PEC1), and the C1 and B2 seams of block IV Parvadeh No. 4 (P4BIVC1 and P4BIVB2), respectively. Size fractions were prepared for mineralogy and liberation degree studies.

3.4.2. Coal Macerals

It is suggested that SEM is a valuable instrument for determining the contents, elements, and minerals in the macerals (Mishra and Singh, 2017). Macerals are divided into three organic groups-vitinite/huminite, liptinite/exinite, and inertinite- and one inorganic group-shale + mineral components [12, 23, 24]. The Parvadeh coal fields have many coal seams, which were petrographically examined. At this step, samples were gathered for the polishing and petrographic sections' examinations. Petrographic sampling and laboratory examinations of polished sections yielded the following results:

The C1 coal seam revealed adequate thickness in the Parvadeh mine complex and adjoining exploration sites. Thus 12 samples of this strata were petrographically studied. The refractive index in the tested samples was between 11 and 14, demonstrating this coal's gloss. The samples have 82–96% organic matter, 2–13% non-caking material, 11–35% ash, and a 15–20 plastometric index. Therefore, this stratum has more coking potential than a C2 coal seam. In well No. 148, fusinite accounts for 2% of non-cakeable minerals. The samples show low fusinite and semi-vitrinite and high vitrinite, indicating sedimentary reduction. This layer's maceral composition is almost 90% vitrinite. The stratum has 4% fusinite and 3–12% semi-vitrinite. Pyrite is sometimes found inside vitrinite as a passive morph of framboidal pyrite. Minerals also include substantial amounts of calcite.

For the B2 coal seam petrographic research, six samples were produced from this stratum. The B2 Layer consists of at least two coal branches at the roof or floor of the seam and a layer of argillite to siltstone in the middle, which is between 20 and 60 cm in thickness. The samples' refractive index ranged from 91 to 95, indicating this coal's gloss and light reflection similarities to layer C1. Due to its composition and thickness, this seam's ash has changed more than others. The samples have a strong plastometric index and good coking potential. These samples vary in content, maceration, and raw material. According to sample analysis, the maceral composition of this stratum is more than 90% vitrinite, 5% semi-vitrinite, 4% fusinite, and a few liptinite macerals. Framboidal pyrite fills vitrinite maceral cavities.

3.4.3. Lithotypes and Microlithotypes

The International Committee for Coal Petrology (1963) describes "lithotype" as a microscopically observable band in humic coals, assessed by physical properties rather than botanical origin. Vitrain, Clarain, Durain, and Fusain are banded bituminous coal lithotypes. The American Society for Testing and Materials (1980) includes in this description attritional coal and any specific mixture of two or more of the five principal lithotypes, such as clarodurain [23]. All Parvadeh coal seams, workable or not, are lumps with vitrinite bands and extensive vertical fractures. Biscuit coal can be found in coal seams B and C. From west to east, the coals are brighter, lumpier, and have visible vitrinite microcrack bands. Secondary calcites fill low-opening microcracks. Occasionally, sulfides such as pyrite and marcasite are discovered within these joints. Field studies of Parvadeh samples in glossy coals with clarain and ultraclean lithotypes of ∑OR were reported to be roughly 90 in most samples and quite low in fusinite and other opaque macerals. Therefore, petrographic analyses and polished section samples of Parvadeh coal seams, notably coal seams such as C and B, reveal that maceral vitrinite is prominent in all samples and that their microlithotype can be named vitrite. Where the amount of fusinite in the samples is close to 10%, the microlithotype of vitrinertite can be applied to the microlithotype of the Parvadeh coalfield. The polarized light microscope showed vitrinite and fusinite macerals in all three samples of coal. The sample is 70–75% vitrinite and 8–15% fusinite. Clay minerals (illite and kaolinite) are the most important tailings minerals in coal samples, forming locked minerals with macerals at 5–15% concentration (Figure 3 G, H, Figure 4 D, F, and I, and Figure 5 C, D, E, and G). Sample carbonate minerals are 5–12%. (Figures 3C and 6E) and the fractions of carbonate crystals are varied from 0.1-2 mm. Quartz is one of the waste minerals, with an abundance of 2–5%. Finally, the samples contain syngenetic and epigenetic pyrite, two sulfide

minerals. Pyrite is one of the main sulfide minerals in the samples and is found in two forms: syngenetic pyrite and epigenetic pyrite. The former's fractions were -0.2 mm in the form of framboidal pyrite in the coal sample and have an abundance of 1-2%. The latter has a 2–3% replacement in texture. Iron oxides (hematite and goethite) were found as impurities on the coal samples' surface.. Pyrite liberation degrees were studied in three fractions: -2 + 10, -0.5 + -2, and -0.5 mm. Table 3 indicates pyrite liberation for block IV Parvadeh No. 4 and east Parvadeh fractions.

Table 3. Degree of the liberation of pyrite and tailings minerals in the Parvadeh area.

PEC1		
Size fractions (mm)	**dl Pyrite (%)**	**dl tailings (%)**
-10 + 2	5	25
-2 + 0.5	38	55
-0.5	70	84
B4C1		
-10 + 2	20	20
-2 + 0.5	45	50
-0.5	70	80
B4B2		
-10 + 2	5	15
-2 + 0.5	24	45
-0.5	65	75

3.5. Petrography

This study shows the mineralogical analyses and Liberation degrees of three samples (Parvadeh (PEC1) and block IV Parvadeh No. 4 (B4C1 and B4B2) mines). Calcite, dolomite, pyrite, and clay minerals are important coalfield minerals. Quartz and iron oxyhydroxides exceeded 2–3%. We found that coals (ash base) contained quartz as isolated, angular grains with variable sizes and were disseminated in organic matter and clay minerals, indicating a detrital sedimentary rock way in the east Parvadeh area and block IV Parvadeh No. 4 Mines (Figure 3 A, C, Figure 4 A, and Figure 5 B, C). Petrographical examinations of coalfields show that vitrinite dominates with fusinite traces (Figure 3. E, Figure 4. F, and Figure 5. A, E). The first type of pyrite is organic, framboidal, -0.02 mm, and 2%. The second variety, epigenetic pyrite, has a frequency of 0–2%, and is found in the sample with a replacement texture. Framboidal aggregate in coals occurs as shown in (Figure 3 B, H, Figure 4 A, B, C, and Figure 5 A, F, H), and massive pyrite forms anhedral to subhedral crystals (Figure 3 D, F, G, Figure 4 F, G, H, I, and Figure 5 A, D, I). Pyrite is generated during peat development or early diagenesis, likely at 25 °C [1, 25, 26]. Pyrite framboid is common in coals and can be found as framboid in organic-rich environments, where the basic role of organic processes is similar to biogenic sulfate reduction. However, organic molecules and polymer matrix regulate growth, crystal size, shape, particle aggregation, and metal solubility [27]. It was experimentally revealed that oil was generated from dead bacteria and their waste products with precipitated iron sulfides during anaerobic organic matter decomposition [27]. Coal liberation from related minerals was measured using microscopic particle counting. The liberation degree is calculated for the east Parvadeh (PEC1) and block IV Parvadeh No. 4 (B4C1 and B4B2) mines, respectively. Thin-polished and polished sections of fractioned samples (-10 + 2 mm, -2 + 0.5 mm, and -0.5 mm) were investigated by a ZEISS Axioplan 2 polarised light microscope with reflected and transient light to determine liberation degree. Table 3 displays some liberation degree studies. Frequency studies demonstrate that larger fractions of minerals are locked together, and generally many minerals are locked together (Figure 3 A, C, and D). Coal-pyrite-quartz, coal-quartz-calcite, and coal-pyrite-clay mineral systems lock (Figure 3 F, G, Figures 4 D, F, G, H, and Figures 5 C, D, F, G). As particle size decreases, locking generally includes coal-quartz, coal-calcite, coal-pyrite, and coal-clay minerals (Figure 3 I, Figure 4 H, I and Figures 5 G, H, and I). Primary tailings minerals such as quartz and calcite are trapped by the coal edges, in which they are sometimes inclusions.

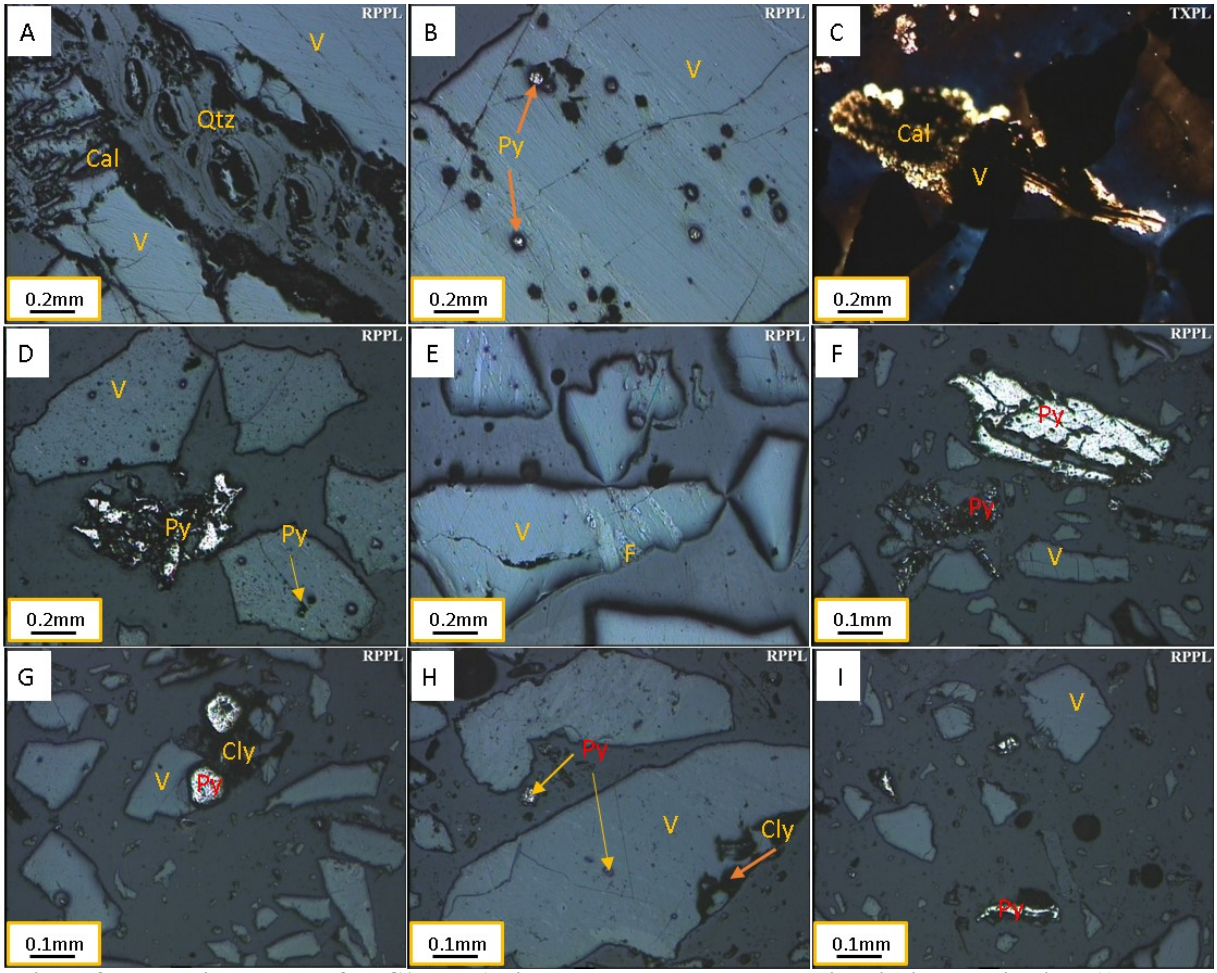

Figure 3. Photomicrographs of PEC1 coal. All images are taken under polarized incident white light A) space-filling of quartz (Qtz) and calcite (Cal) in vitrinite (V), B) pyrite (Py) inclusions in vitrinite, C) association of calcite with vitrinite D) Massive pyrite particle associated with pyrite and framboidal pyrite as inclusion in vitrinite, E) fusinite (F) interbanded with vitrinite, F) massive pyrite particle and pyrite associated with vitrinite, G) pyrite and clay (Cly) mineral associated with vitrinite, H) liberated pyrite particle and pyrite and clay minerals associated with vitrinite, I) liberated pyrite and vitrinite particles.

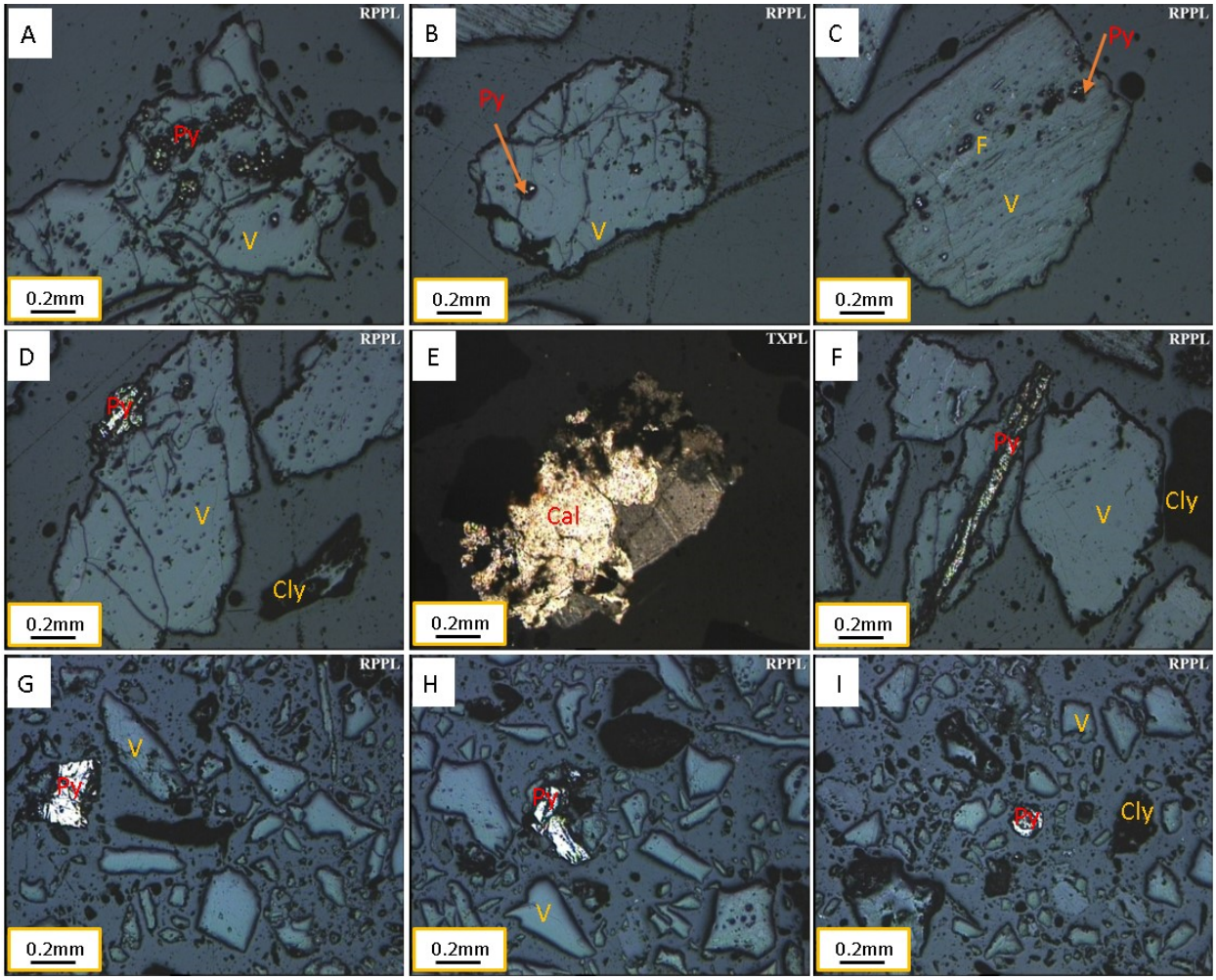

Figure 4. Photomicrographs of B4C1 coal. All images are taken under polarized incident white light. A, B) framboidal pyrite in vitrinite, C) fusinite interband with vitrinite and pyrite inclusions in vitrinite F, G, H) vitrinite particle associated with massive pyrite, I) liberated pyrite, clay minerals, and vitrinite particles.

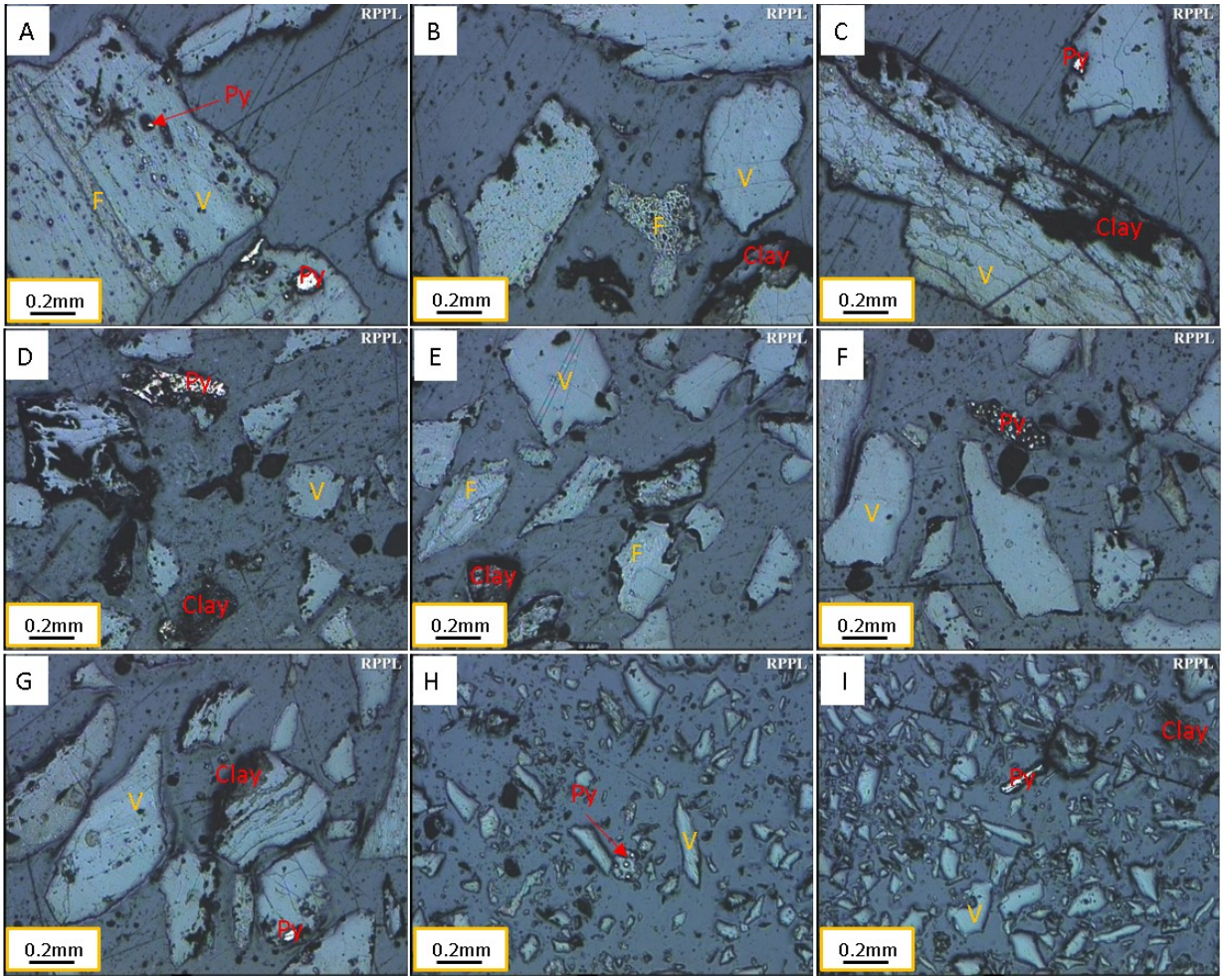

Figure 5. Photomicrographs of B4B2 coal. All images are taken under polarized incident white light A) fusinite interband with vitrinite, (B) calcite and clay filling the fusinite cells, (C) clay minerals and pyrite filling vitrinite, D) pyrite associated with vitrinite and clay minerals, E) fusinite interband with vitrinite and clay minerals associated with vitrinite, F) framboidal pyrite and pyrite inclusions in vitrinite, G, H) clay minerals and pyrite associated with vitrinite, I) liberated pyrite and vitrinite particles.

3.6. Scanning electron microscope (SEM) studies

The coal samples are classified into three types based on their sulfur contents: low-sulfur coals (< 1% S), medium-sulfur coals (=1 to < 3% S), and high-sulfur coals (≥ 3% S) [26]. The sulfur of medium-sulfur coals and high-sulfur coals has two primary sources: plant materials and seawater sulfate. Electron microscopy studies were performed on a polished section of PEC1, P4B4B2, and P4B4C1 coal seams with a fraction of -10 + 2, -2 + 0.5, and -0.5 mm, respectively. The mineralogical compositions of the samples and SEM images of sulfur and sulfate minerals are displayed in Table 1 and Figures 6-8 separately. Images produced by QBSD return electrons show areas with heavier elements in a lighter color. SEM-EDS analyses were carried out utilizing an ETH of 20 kV and a WD of 15 mm. Pyrite is locked in the coal matrix with calcite and dolomite (Figure 6 A, B, and D, and Figure 7 A and B, and Figure 8 G). Some iron oxide is mainly free (Figure 7 D and Figure 8 E), and some clay minerals are locked in the samples (Figure 6 G, H, Figure 7 H, and Figure 8 A, C, F, and I). A significant amount of free pyrite is observed. In the samples, other minerals, including pyrrhotite, ankerite, dolomite, barite, smithsonite, galena, quartz, and apatite, are presented in small amounts (Figure 6, G, and H and Figure 7 A, B, and H). As demonstrated by this study and prior investigation, these samples, as commonly observed, contain high levels of altered pyrite and the formation of secondary iron sulfate minerals under humid conditions [26, 28]. Iron oxides and hydroxides are seen as surface impurities in the sample. In microscopic studies, the non-metallic minerals in the sample that reflect light are considered as waste minerals.

3.7. Gangue mineralogy

Parvadeh coal pyrite morphologies: (1) veinlet-shaped pyrite (Figures 4 F and 8 D) and (2) framboidal pyrite are syngenetic types and the maximum pyrite shape in Parvadeh coal samples (Figure 6 A) and occur primarily as inclusions. Framboidal pyrite particles and clusters are mainly found in organic matter (maceral) and clay mineral aggregates (Figure 8 E, H). (3) Most pyrites are enormous framboidal syngenetic bodies (Figure 7 B). The sulfate-rich solution infiltrated and circulated the coal beds, forming the cleat/fracture pyrite infillings at late diagnostic and epigenetic stages [1, 2]. Pore-waters and/or inter-seam solutions may cause moveables of sulfate-rich solution and allow filtered solutions to enter peat beds beneath altered tuff layers during late syngenetic and diagenetic stages [1]. Calcite, dolomite, and clay minerals in Parvadeh bind 0.2-mm pyrite particles (Figure 8 C, G, and I). Pyrite particles are crystal aggregations; therefore, sulfide mineral sedimentation should begin at several nucleation sites before coal-forming compaction [29]. Bacteria reduce sulfates to form these pyrites. Pyritized bacteria are rarely found. It is discovered pyritized bacteria species in high-sulfur coals from the Wuda and Zhaotong coalfields, China, and suggested that bacteria and algae may have helped produce them [30], where pyritized bacteria described in Chongqing's Nantong Coalfield's high-sulfur coals. If coal samples are broken naturally, watch for coin-shaped pyrite circles. Illite, quartz, calcite, dolomite, ankerite, hematite, apatite, and galena are the main waste minerals (Figure 8 B, E, G, and H). Inorganic Parvadeh materials, like coal seams worldwide, are mostly clay minerals (illite). In detrital coal samples, quartz is the most important mineral. Aluminosilicate syngenetic alteration can also produce this mineral [31]. Pyrite forms one micron-sized euhedral and one framboid crystal in marine sediments [32]. Pyrite and quartz in cleaned coals do not diminish during Parvadeh coal washing. Calcite is a characteristic Parvadeh epigenetic cleat, fracture, and/or cell-filling carbonate mineral (Figure 6B). It degrades easily in peat's acidic environment and emerges as detrital particles [31]. The coal preparation plant removes calcite from the coal supply, which was not separable in concentrate. An X-ray diffractometer studied coal sample ash to detect minerals (XRD). All samples had quartz, illite, hematite, and anhydrite. XRD plots of ash samples PEC1, B4C1, and B4B2 reveal that sample PEC1 has the lowest illite content and the highest anhydrite and hematite content (Figure S3). XRD plots reveal ash sample B4B2 has the most illite and quartz. Gypsum is the main mineral in coal samples that decomposes with heat and becomes anhydrite via water loss [33]. Table S4 shows the major and minor minerals in PEC1, B4C1, and B4B2 based on transmission-reflective light microscopy, SEM, and XRD. Back-scattered phase separation color images show fine pyrite minerals and their relationship with macerals and micro-minerals.

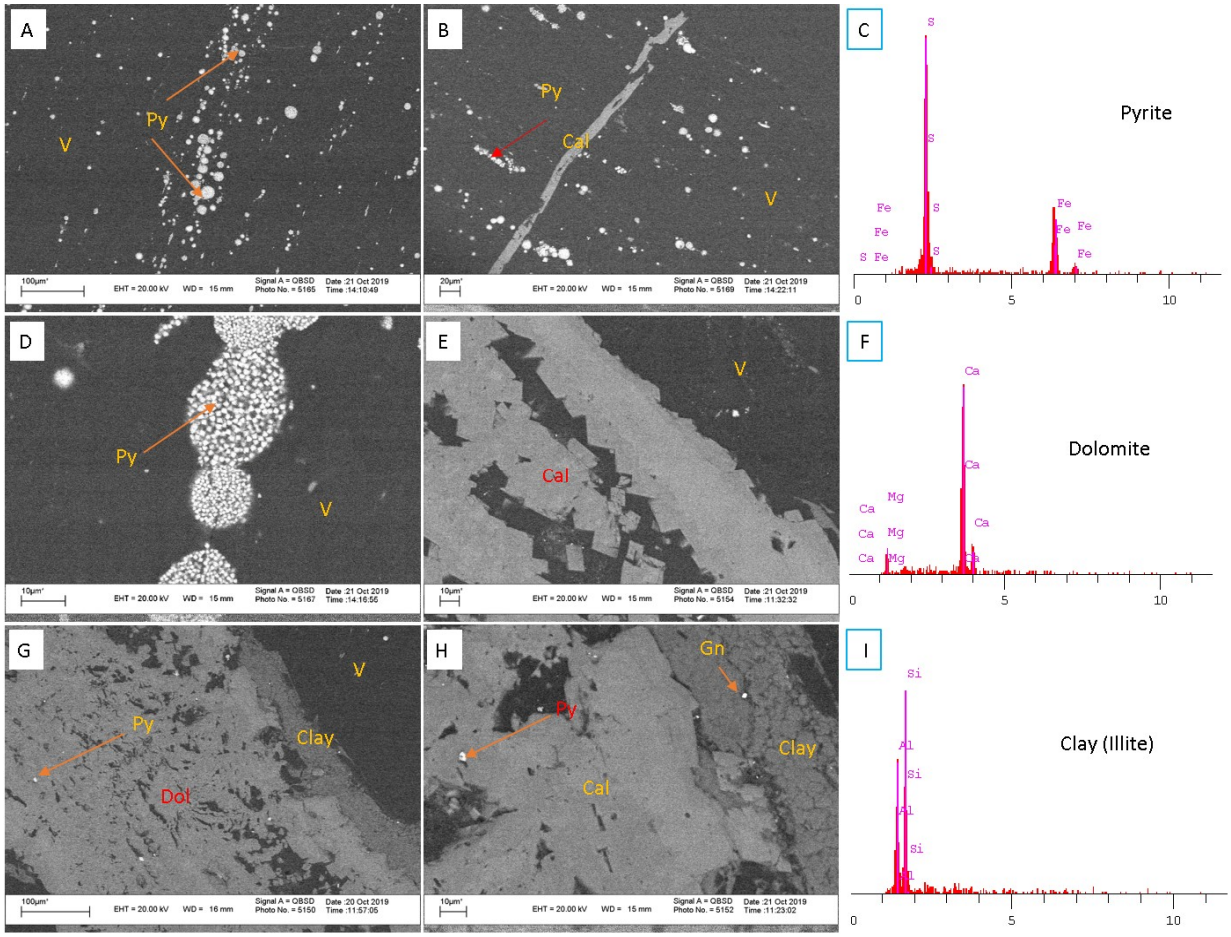

Figure 6. SEM backscattered images and EDX data in the PEC1 coal samples A) distribution of framboidal pyrite in vitrinite, B) calcite as space-filling in vitrinite, C) pyrite EDX data, D) framboidal pyrite in vitrinite, E) euhedral calcite crystals in vitrinite, F) dolomite (Dol) EDX data, G) dolomite and Clay mineral (illite) associated with vitrinite, H) pyrite inclusion in calcite and galena (Gn) Clay mineral (illite), I) illite EDX data.

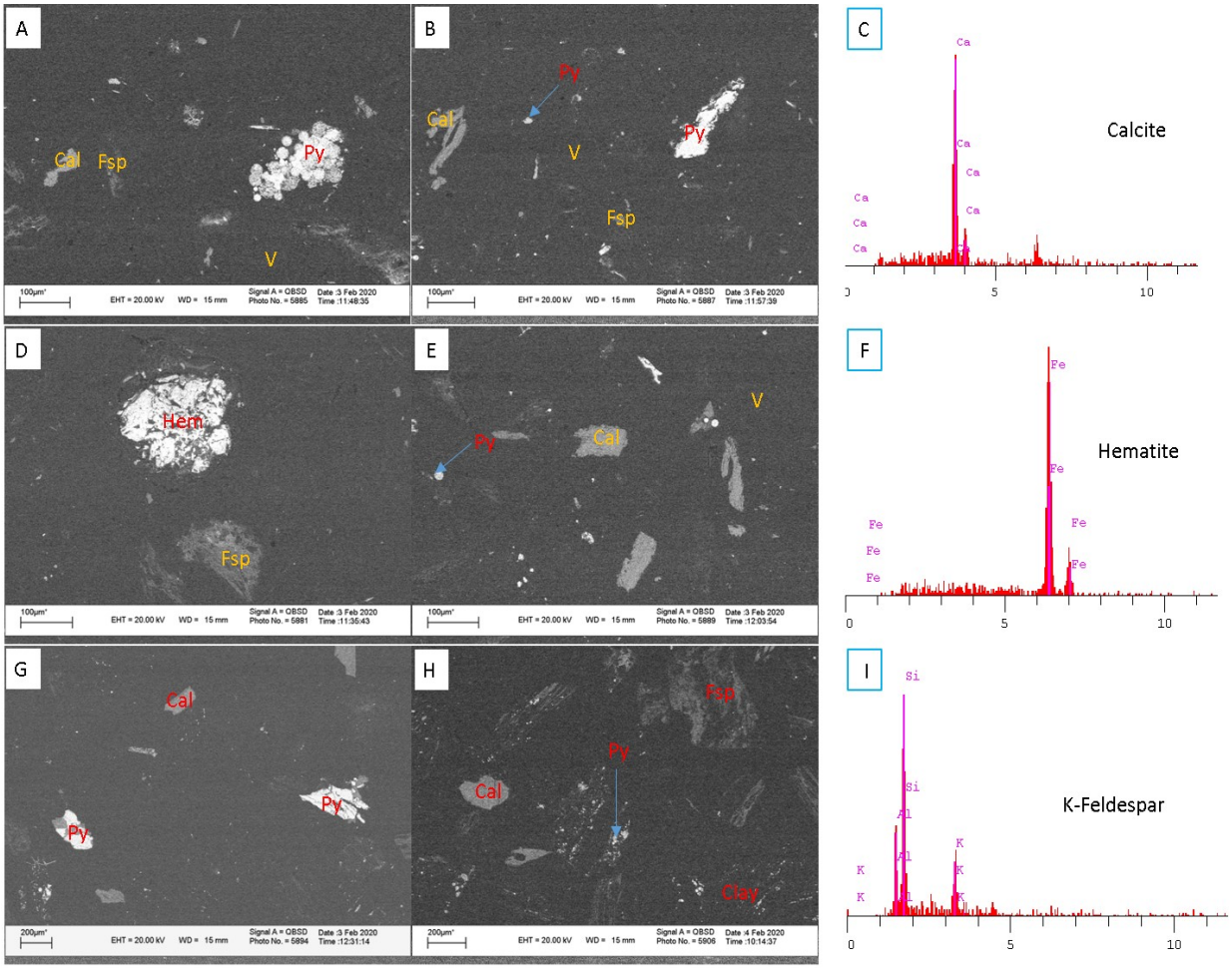

Figure 7. SEM back-scattered images and EDX data in the B4C1 coal samples, A) framboidal pyrite in vitrinite, B) massive particle pyrite, C) calcite EDX data, D) massive particle hematite (Hem), E) calcite particle, F) hematite EDX data, G) massive pyrite particles and calcite particle, H) Framboidal pyrite as inclusion in vitrinite, calcite, and K-feldspar (Fsp) particles, I) K-feldspar EDX data.

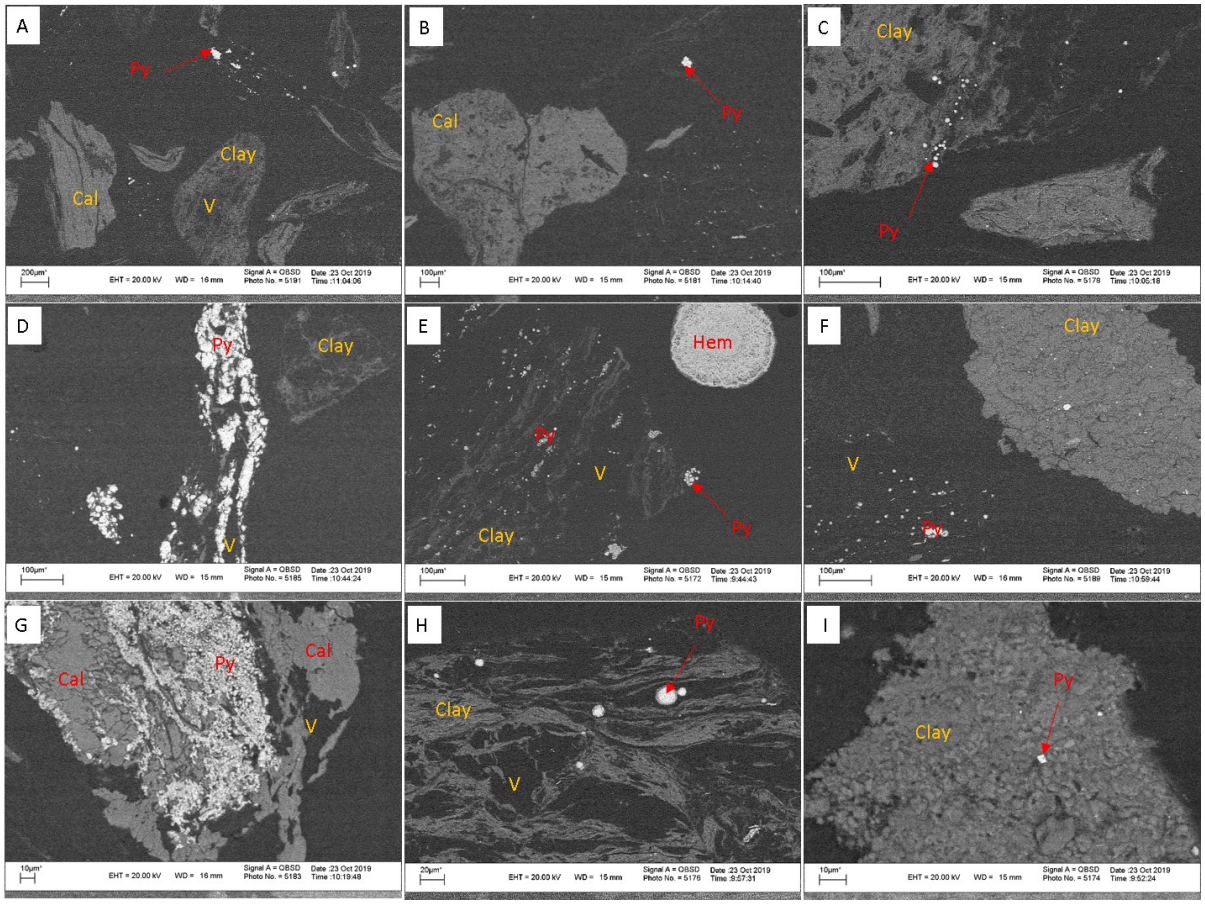

Figure 8. SEM back-scattered images in the B4B2 coal samples, A) pyrite inclusions in vitrinite, B) calcite particle, C) framboidal pyrite in clay mineral, D) massive pyrite particle associated with vitrinite, E) hematite particle, framboidal pyrite, and clay associated with vitrinite, F) clay mineral particle and distribution of fine pyrite in vitrinite, G) pyrite and calcite associated with vitrinite, H) framboidal pyrite in vitrinite, I) pyrite inclusion in clay mineral.

4. Conclutions

Mineralogical studies have shown that the mineralogical composition of the three sample types of Parvadeh coalfield (B4B2, B4C1, and PEC1) are very similar. The dominant minerals in coal samples include clay, pyrite, calcite, dolomite, quartz, and hematite-goethite. Pyrite is observed in two types in the samples. The first type of pyrite is of organic origin, which is smaller than 0.1 mm in size and is seen as a framboid in the samples (syngenetic type) and has about 1-2%. The second type of pyrite is massive (epigenetic), and its approximate amount is 2–3%. Framboidal pyrites are fine-crystalline and commonly formed during peatification processes. The accumulation of pyrite in coal can be due to the abundant presence of iron-rich minerals in sediments during peatification. Epigenetic pyrite is much more dominant and forms in cracks, cavities, and cleats. Vitrinite is the most abundant maceral in the samples and makes up about 70% to 80% of the samples. Fusenite, with an abundance of about 8–15%, is another prominent maceral in samples. Clay minerals (mostly illite) are present in the sample in amounts ranging from 8–10%. Carbonate minerals (calcite and dolomite), which are approximately 5-8% in the samples, are other vital minerals. The dimensions of carbonate crystals are varied, and the dimensions range from larger than 2 mm to less than 0.1 mm. Carbonate inclusions have been observed inside the coal. Quartz is a typical waste mineral and is about 3-5 percent abundant. X-ray diffraction studies on ash samples showed that sample PEC1 contained the most hematite and anhydrite, and sample B4B2 contained the highest amounts of illite and quartz. The liberation degree of pyrite and tailings minerals in the Parvadeh area sample is related to the type of waste minerals in the sample. Samples PEC1 and B4C1 have a better liberation degree because they have less clay minerals and quartz.

Acknowledgments

The authors are grateful to acknowledge the IMIDRO (Iranian Mines and Mining Industries Development and Renovation Organization) that supported this study. The authors would like to thank the TCMC, IMPRC, and University of Tehran for the Research Council that also supported this work.

References

[1]. Karayiğit, A.İ., Littke, R., Querol, X., Jones, T., Oskay, R.G., and Christanis, K. (2017). The Miocene coal seams in the Soma Basin (W. Turkey): Insights from coal petrography, mineralogy and geochemistry. International Journal of Coal Geology, 173, 110-128..

[2]. Dai, S., and Finkelman, R.B. (2018). Coal as a promising source of critical elements: Progress and future prospects. International Journal of Coal Geology, 186, 155-164.

[3]. Dai, S., Bechtel, A., Eble, C.F., Flores, R. M., French, D., Graham, I.T., and O'Keefe, J.M. (2020). Recognition of peat depositional environments in coal: A review. International Journal of Coal Geology, 219, 103383.

[4]. Duan, P., Wang, W., Liu, X., Sang, S., Ma, M., and Zhang, W. (2019). Differentiation of rare earth elements and yttrium in different size and density fractions of the Reshuihe coal, Yunnan Province, China. International Journal of Coal Geology, 207, 1-11.

[5]. Finkelman, R. B., Dai, S., and French, D. (2019). The importance of minerals in coal as the hosts of chemical elements: A review. International Journal of Coal Geology, 212, 103251.

[6]. Li, D., Tang, Y., Deng, T., Chen, K., Liu, D., and Cheng, F. (2008). Mineralogy of the no. 6 coal from the Qinglong Coalfield, Guizhou Province, China. Energy exploration and exploitation, 26 (6): 347-353.

[7]. Jorjani, E., Rezai, B., Vossoughi, M., and Osanloo, M. (2004). Desulfurization of Tabas coal with microwave irradiation/peroxyacetic acid washing at 25, 55 and 85 C. Fuel, 83 (7-8): 943-949.

[8]. Wheelock, T.D., and Markuszewski, R. (1984). Coal preparation and cleaning. The science and technology of coal and coal utilization, 47-123.

[9]. Singh, P.K., Singh, A.L., Kumar, A., and Singh, M.P. (2013). Control of different pyrite forms on desulfurization of coal with bacteria. Fuel, 106, 876-879.

[10]. Geboy, N.J., Engle, M.A., and Hower, J.C. (2013). Whole-coal versus ash basis in coal geochemistry: a mathematical approach to consistent interpretations. International Journal of Coal Geology, 113, 41-49.

[11]. Xu, N., Finkelman, R.B., Xu, C., and Dai, S. (2020). What do coal geochemistry statistics really mean?. Fuel, 267, 117084.

[12]. Kwiecińska, B., Pusz, S., and Valentine, B.J. (2019). Application of electron microscopy TEM and SEM for analysis of coals, organic-rich shales and carbonaceous matter. International Journal of Coal Geology, 211, 103203.

[13]. Jorjani, E., Chelgani, S.C., and Mesroghli, S. (2007). Prediction of microbial desulfurization of coal using artificial neural networks. Minerals Engineering, 20 (14): 1285-1292.

[14]. Llovet, X., Moy, A., Pinard, P.T., and Fournelle, J.H. (2021). Reprint of: Electron probe microanalysis: A review of recent developments and applications in materials science and engineering. Progress in Materials Science, 120, 100818.

[15]. Ahangaran, D.K., Afzal, P., Yasrebi, A.B., Wetherelt, A., Foster, P.J., and Darestani, R.A. (2011). An evaluation of the quality of metallurgical coking coal seams within the north block of Eastern Parvadeh coal deposit, Tabas, Central Iran. Journal of Mining and Metallurgy A: Mining, 47 (1): 9-24.

[16]. Zamansani, N., Rajabzadeh, M.A., Littke, R., Zieger, L., and Baniasad, A. (2019). Organic petrology and geochemistry of Triassic and Jurassic coals of the Tabas Basin, Northeastern/Central Iran. International Journal of Coal Science & Technology, 6, 354-371.

[17]. NAEIMI, G.N., Saeidi, A., Aghanabati, A., GHOREYSHI, M., and Ghasemi, M.R. (2010). Geohistory Analysis of the Tabas Block (Abdoughi-Parvadeh Basins) as Seen from the Late Triassic through Early Cretaceous Subsidence Curves.

[18]. Moosavirad, S.M., Rasouli, J., Janardhana, M.R., Moghadam, M.R., and Shankara, M. (2013). Petrographic, mineralogy, and geochemistry of coals of Pabedana, Kerman Province, Central Iran. Arabian Journal of Geosciences, 6, 3623-3634.

[19]. Moore, F., and Esmaeili, A. (2012). Mineralogy and geochemistry of the coals from the Karmozd and Kiasar coal mines, Mazandaran province, Iran. International journal of coal geology, 96, 9-21.

[20]. Afzal, P., Alhoseini, S. H., Tokhmechi, B., Ahangaran, D. K., Yasrebi, A. B., Madani, N., and Wetherelt, A. (2014). Outlining of high quality coking coal by concentration–volume fractal model and turning bands simulation in East-Parvadeh coal deposit, Central Iran. International Journal of Coal Geology, 127, 88-99.

[21]. Dai, S., Jiang, Y., Ward, C.R., Gu, L., Seredin, V.V., Liu, H., and Ren, D. (2012). Mineralogical and geochemical compositions of the coal in the Guanbanwusu Mine, Inner Mongolia, China: Further evidence for the existence of an Al (Ga and REE) ore deposit in the Jungar Coalfield. International Journal of Coal Geology, 98, 10-40.

[22]. Kozlov, A., Svishchev, D., Donskoy, I., Shamansky, V., and Ryzhkov, A. (2015). A technique proximate and ultimate analysis of solid fuels and coal tar. Journal of Thermal analysis and Calorimetry, 122, 1213-1220.

[23]. Mishra, V., and Singh, K.N. (2017). Microstructural relation of macerals with mineral matter in coals from Ib valley and Umaria, Son-Mahanadi basin, India. International Journal of Coal Science & Technology, 4, 191-197.

[24]. Singh, M.P., and Singh, P.K. (1995). Mineral Matter in the Lrajmahal Coals: Study Through Incident Light Microscopy and Scanning Electron Micrography. Geological Society of India, 46 (5): 557-564.

[25]. Dai, S., Zhang, W., Ward, C.R., Seredin, V.V., Hower, J.C., Li, X., and Zhou, D. (2013). Mineralogical and geochemical anomalies of late Permian coals from the Fusui Coalfield, Guangxi Province, southern China: influences of terrigenous materials and hydrothermal fluids. International Journal of Coal Geology, 105, 60-84.

[26]. Chou, C. L. (2012). Sulfur in coals: A review of geochemistry and origins. International journal of coal geology, 100, 1-13.

[27]. Rickard, D. (1997). Kinetics of pyrite formation by the H2S oxidation of iron (II) monosulfide in aqueous solutions between 25 and 125 C: The rate equation. Geochimica et Cosmochimica Acta, 61 (1): 115-134.

[28]. Erarslan, C., Örgün, Y., and Balcı, N. (2020). Source and distribution of pyrite and inorganic sulfur isotopes in the Saray and Pınarhisar Coalfields, North Thrace Basin, Turkey. International Journal of Coal Geology, 227, 103533.

[29]. Southam, G., Donald, R., Röstad, A., and Brock, C. (2001). Pyrite discs in coal: Evidence for fossilized bacterial colonies. Geology, 29 (1): 47-50.

[30]. Dai, S., Ren, D., Zhou, Y., Chou, C. L., Wang, X., Zhao, L., and Zhu, X. (2008). Mineralogy and geochemistry of a superhigh-organic-sulfur coal, Yanshan Coalfield, Yunnan, China: Evidence for a volcanic ash component and influence by submarine exhalation. Chemical Geology, 255 (1-2): 182-194.

[31]. Dai, S., Zou, J., Jiang, Y., Ward, C.R., Wang, X., Li, T., and Zhou, D. (2012). Mineralogical and geochemical compositions of the Pennsylvanian coal in the Adaohai Mine, Daqingshan Coalfield, Inner Mongolia, China: Modes of occurrence and origin of diaspore, gorceixite, and ammonian illite. International Journal of Coal Geology, 94, 250-270.

[32]. Goodarzi, F. (2002). Mineralogy, elemental composition and modes of occurrence of elements in Canadian feed-coals. Fuel, 81 (9): 1199-1213.

[33]. Rajabzadeh, M. A., Ghorbani, Z., and Keshavarzi, B. (2016). Chemistry, mineralogy and distribution of selected trace-elements in the Parvadeh coals, Tabas, Iran. Fuel, 174, 216-224.

مطالعات کانی شناسی و خصوصیت سنجی با هدف فرآیند گوگردزدایی زغال سنگ در بزرگترین حوزه‌ی زغالسنگ ایران

سجاد جان‌نثار ملکوتی[1*]، هادی عبداللهی[2]، ضیاءالدین پورکریمی[2]، بهروز کریمی شهرکی[3] ، مهدی رحیمی[3]، محمدرضا شهبازی[2] و احمد رحمانیان[2]

۱- مجتمع معادن زغال سنگ طبس (TCMC)، سازمان توسعه و نوسازی معادن و صنایع معدنی ایران (ایمیدرو)، طبس، ایران

۲- دانشکده مهندسی معدن، دانشکده فنی، دانشگاه تهران، تهران، ایران

۳- مرکز تحقیقات فرآوری مواد معدنی ایران، ایران

ارسال ۲۰۲۲/۱۲/۱۹، پذیرش ۲۰۲۳/۰۲/۲۸

* نویسنده مسئول مکاتبات: s.jannesar114@gmail.com

چکیده:

معادن پروده IV و پروده شرقی دو معدن ا صلی تولید زغال سنگ در حوزه‌ی زغال‌سنگ طبس می‌با شند. از آنجایی که مطالعات ن شان داد که لایه‌های C1 و B2 مهمترین جبهه کار در نواحی پروده ۴ و پروده شـرقی هسـتند، این پژوهش بر روی این دو لایه کاری قابل اسـتخراج متمرکز شـده اسـت. در این نمونه ها، پیریت همزمان به صورت دانه تمشکی در ماسرال‌ها موجود است. کاهش محتوای گوگرد مخصوصاً زمانی که ذرات پیریت ریزدانه شده و با در ساختار ماسرال زغال سنگ ر شد می‌کنند، بـسیار سخت و چالش برانگیز ا ست. میزان گوگرد اندازه‌گیری شده در لایه‌های C1 و B2 به ترتیب از ۰,۹۸٪ تا ۵,۵۷٪ و از ۰,۷۳٪ تا ۵,۲۵٪ با میانگین ۲,۳۹٪ و ۲,۵٪ متغیر اسـت. از روشـی به منظور پیش‌بینی چگونگی گوگردزدایی از زغال‌سـنگ لایه‌های C1 و B2 معادن پروده IV و C1 معدن پروده شرقی در حوزه‌ی زغال‌سنگ طبس استفاده شد. نتایج شواهد جدیدی برای حضور پیریت و کانی‌های رسی در ناحیه‌ی زغال‌سنگی مذکور و شناسایی روشی برای پیش‌بینی گوگردزدایی زغال سنگ با روش‌های مر سوم فرآوری و مقرون‌به صرفه ارائه کرده‌اند. ا ستراتژی کانه‌آرایی زغال‌سنگ در کارخانه‌های زغال شویی شرکت گسترش و نوسازی معادن خاورمیانه، پروده و احیا سپاهان نه به دلیل دفع مواد معدنی و پیریت، بلکه به سبب کاهش محتوای بیشتر اجزای غیرآلی زغال می‌باشد.

کلمات کلیدی: کانی‌شناسی زغال سنگ، گوگردزدایی زغال سنگ، پیریت فرامبوئیدال، کارخانه زغال شویی.